Vision Research 49 (2009) 637–647

Contents lists available at ScienceDirect

Vision Research

journal homepage: www.elsevier.com/locate/visres

Retinal ganglion cell population in adult albino and pigmented mice: A computerized analysis of the entire population and its spatial distribution

M. Salinas-Navarro [a,1], M. Jiménez-López [a,1], F.J. Valiente-Soriano [a], L. Alarcón-Martínez [a], M. Avilés-Trigueros [a], S. Mayor [a], T. Holmes [b], R.D. Lund [c], M.P. Villegas-Pérez [a], M. Vidal-Sanz [a,*]

[a] Laboratorio de Oftalmología Experimental, Facultad de Medicina, Universidad de Murcia, E-30100 Murcia, Spain
[b] Catherine McCauley Centre, University College Dublin, Dublin, Ireland
[c] Casey Eye Institute, Oregon Health Sciences University, Portland, OR, USA

ARTICLE INFO

Article history:
Received 25 November 2008
Received in revised form 14 January 2009

Keywords:
Retinal ganglion cells
Visual streak
Fluorescent tracers
Retrograde labeling
Image analysis
Computerized analysis

ABSTRACT

In adult Swiss albino and C57 pigmented mice, RGCs were identified with a retrogradely transported neuronal tracer applied to both optic nerves (ON) or superior colliculi (SCi). After histological processing, the retinas were prepared as whole-mounts, examined and photographed under a fluorescence microscope equipped with a motorized stage controlled by a commercial computer image analysis system: Image-Pro Plus® (IPP). Retinas were imaged as a stack of 24-bit color images (140 frames per retina) using IPP with the Scope-Pro plug-in 5.0 and the images montaged to create a high-resolution composite of the retinal whole-mount when required. Single images were also processed by specific macros written in IPP that apply a sequence of filters and transformations in order to separate individual cells for automatic counting. Cell counts were later transferred to a spreadsheet for statistical analysis and used to generate a RGC density map for each retina. Results: The mean total numbers of RGCs labeled from the ON, in Swiss (49,493 ± 3936; $n = 18$) or C57 mice (42,658 ± 1540; $n = 10$) were slightly higher than the mean numbers of RGCs labeled from the SCi, in Swiss (48,733 ± 3954; $n = 43$) or C57 mice (41,192 ± 2821; $n = 42$), respectively. RGCs were distributed throughout the retina and density maps revealed a horizontal region in the superior retina near the optic disk with highest RGC densities. In conclusion, the population of mice RGCs may be counted automatically with a level of confidence comparable to manual counts. The distribution of RGCs adopts a form of regional specialization that resembles a horizontal visual streak.

1. Introduction

The adult rodent primary visual pathway has been widely used to investigate anatomical, functional and behavioral aspects of the mammalian central nervous system regeneration (Avilés-Trigueros, Sauvé, Lund, & Vidal-Sanz, 2000; Sasaki et al., 1996; Vidal-Sanz, Avilés-Trigueros, Whiteley, Sauvé, & Lund, 2002; Vidal-Sanz, Bray, Villegas-Perez, Thanos, & Aguayo, 1987; Vidal-Sanz, Villegas-Pérez, Bray, & Aguayo, 1993; Whiteley, Sauvé, Avilés-Trigueros, Vidal-Sanz, & Lund, 1998), degeneration (Agudo et al., 2008; Agudo et al., 2009; Chidlow, Casson, Sobrado-Calvo, Vidal-Sanz, & Osborne, 2005; Lafuente, Villegas-Pérez, Sellés-Navarro, et al., 2002; Lund et al., 2007; Sellés-Navarro, Villegas-Pérez, Salvador-Silva, Ruiz-Gomez, & Vidal-Sanz, 1996; Villegas-Perez, Lawrence, Vidal-Sanz, Lavail, & Lund, 1998; Villegas-Perez, Vidal-Sanz, Bray, & Aguayo, 1988; Villegas-Perez, Vidal-Sanz, & Lund, 1996; Villegas-Perez, Vidal-Sanz, Rasminsky, Bray, & Aguayo, 1993; Wang, Villegas-Pérez, Vidal-Sanz, & Lund, 2000) and neuroprotection (Avilés-Trigueros et al., 2003; Lafuente López-Herrera, Mayor-Torroglosa, Miralles de Imperial, Villegas-Pérez, & Vidal-Sanz, 2002; Lafuente et al., 2002; Lund et al., 2007; Mayor-Torroglosa et al., 2005; Vidal-Sanz et al., 2007; Vidal-Sanz et al., 2007; Vidal-Sanz et al., 2000).

In rodents, like in most mammals, RGCs project to a number of central regions known as retino-recipient targets including the suprachiasmatic nuclei, the accessory optic nuclei, the pretectal nuclei, the ventral lateral geniculate nuclei, the dorsal lateral geniculate nuclei, and the superior colliculi (Rodiek, 1979). The vast majority of RGCs project to the superior colliculi (Lund, 1965; Perry, 1981) where RGCs axons deploy in a very precise topographic manner (Linden & Perry, 1983; Sauvé, Girman, Wang, Lawrence, & Lund, 2001; Sauvé, Girman, Wang, Keegan, & Lund, 2002), but to date the exact magnitude of this projection has only recently been examined in adult rats (Salinas-Navarro et al., 2009). Within the rodent retina, the RGC population is distributed throughout in a central-peripheral gradient and some authors have

* Corresponding author. Fax: +34 968 36 39 62.
E-mail address: ofmmv01@um.es (M. Vidal-Sanz).
[1] These authors have contributed equally towards this work.

0042-6989/$ - see front matter © 2009 Elsevier Ltd. All rights reserved.
doi:10.1016/j.visres.2009.01.010

found a region with highest RGC density in the superior retina, mainly within the superior temporal region of mice (Drager & Olsen, 1981; Jakobs, Libby, Ben, John, & Masland, 2005; Jeon, Strettoi, & Masland, 1998), Syrian hamster (Métin, Irons, & Frost, 1995) and rat (Dreher, Sefton, Ni, & Nisbett, 1985; Fukuda, 1977; Jeffery, 1985; Perry, 1981; Reese & Cowey, 1986; Schober & Gruschka, 1977), but whether they adopt some form of regional specialization has been controversial (Danias et al., 2002; Danias et al., 2003; Reese, 2002; Salinas-Navarro et al., 2009). Such concept is important because the distribution of RGCs in the retina reflect the regional specialization and resolution of the visual system (Drager & Hubel, 1976; Prusky, Harker, Douglas, & Whishaw, 2002).

Adult Swiss and C57BL/6J strains of mice with non-pigmented and pigmented eyes, respectively, are usually employed for experimental models of injury-induced RGC loss and its prevention, thus it was of interest to determine, as a reference for future studies, the total number of RGCs in these mice, the number of RGCs projecting to the superior colliculi and their regional distribution within the retina. In the present study we have taken advantage of retrogradely transported tracers to identify the entire RGC population and used an automated methodology to count labeled RGCs (Danias et al., 2002; Nadal-Nicolás et al., 2009; Salinas-Navarro et al., 2009; Vidal-Sanz, De la Villa, et al., 2007; Vidal-Sanz, Salinas-Navarro, et al., 2007). We report the numbers of RGCs that give rise to the retinofugal projection in Swiss and Adult C57BL/6J mice, as well as the numbers of RGCs that contribute to the retinotectal projection, providing additional direct evidence for the massive contralateral projection in the retinofugal system of adult mice (Drager & Olsen, 1981; Lund, 1965). The analysis of the RGC spatial distribution, adds to the existing literature showing a horizontally oriented high-density region of RGCs in the dorsal retina, resembling a visual streak. These data provide necessary background information for studying the effects of genetic and induced changes associated with mouse disease models of glaucoma, and the photoreceptor degenerations [part of this work have been presented in abstract form (Salinas-Navarro et al., 2005; Vidal-Sanz, Salinas-Navarro, et al., 2007; Villegas-Pérez et al., 2006).

2. Methods

2.1. Animals and anesthesia

Experiments were performed on adult male albino Swiss ($n = 34$) and pigmented C57BL/6N ($n = 26$) mice, (weighing 37 and 31 g, respectively) obtained from the breeding colony of the University of Murcia (Murcia, Spain). Mice were housed in temperature and light controlled rooms with a 12 h light/dark cycle and had food and water ad libitum. Light intensity in the animal room was programmed to be of 24 lux, depending on the location of the animal cage within the rack, the intensity varied from 9 to 24 lux.

When animal manipulations were performed, the "Principles of laboratory animal care" (NIH publication No. 85–23, revised 1985), the OPRR Public Health Service Policy of the Human Care and the Use of Laboratory Animals (revised 1986) and the US Animal Welfare Act, as amended, were followed, as well as our institutional guidelines, European Union regulations for the use of animals in research and the ARVO statement for the use of animals in ophthalmic and vision research. In addition, additional measures were taken to minimize pain or discomfort.

All surgical manipulations were done under general anesthesia induced with an intraperitoneal (i.p.) injection of ketamine (70 mg/kg, Ketolar®, Parke-Davies, S.L., Barcelona, Spain) and xylazine (10 mg/kg, Rompún®, Bayer, S.A., Barcelona, Spain). While recovering from anesthesia, mice were placed in their cages, and an ocular ointment containing neomycin and prednisone (Oftalmolosa Cusí Prednisona-Neomicina®; Alcon S.A., Barcelona, Spain) was applied on the cornea to prevent corneal desiccation. Animals were euthanized with an i.p. injection of an overdose of pentobarbital (Dolethal Vetoquinol®, Especialidades Veterinarias, S.A., Alcobendas, Madrid, Spain).

2.2. Retrograde tracing

In the ganglion cell layer of the rodent retina there are RGC and displaced amacrine cell populations in similar proportions (Drager & Olsen, 1981; Perry, 1981; Perry, Henderson, & Linden, 1983), as well as a small number of displaced horizontal cells (Silveira, Picanço-Diniz, & Oswaldo-Cruz, 1989; Silveira, Yamada, & Picanço-Diniz, 1989). For instance, in the mouse retina approximately 59% of the neurons in the GC layer are displaced amacrine cells (Drager & Olsen, 1981; Jeon et al., 1998; Schmidt, Vitral, & Linden, 2001). Thus, a well established method to identify RGCs has consisted on the application of retrogradely transported tracers to their main target regions in the brain or to their optic tracts or nerves (Lafuente López-Herrera, et al., 2002; Peinado-Ramon, Salvador, Villegas-Perez, & Vidal-Sanz, 1996; Sellés-Navarro et al., 1996; Vidal-Sanz, Lafuente, Mayor, de Imperial, & Villegas-Pérez, 2001). One tracer proven reliable and efficient for the visual system is FluoroGold™ (2-Hydroxystilbene-4,4′-dicarboxamidine bis (methanesulfonate)) (Salinas-Navarro et al., 2009) or its equivalent hydroxystilbamidine methanesulfonate (OHSt) a small (472,53 kDa Mw) molecule (Molecular Probes, Leiden, The Netherlands) with similar fluorescent and tracer properties to fluorogold (Cheunsuang & Morris, 2005).

2.2.1. Tracing from the optic nerve

To label the bulk of the retinofugal projection from each retina the optic nerves were transected intraorbitally in 10 Swiss and in 5 C57 mice, a small pledget of gelatin sponge soaked in a solution containing 10% OHSt (Molecular Probes, Leiden, The Netherlands) in 0.9% NaCl and 10% dimethyl sulphoxide (DMSO) was applied to the ocular stump of the cut optic nerve, approximately 1 mm from the optic disk following previously described methods that are standard in our laboratory (Lafuente López-Herrera, et al., 2002; Salinas-Navarro et al., 2009; Vidal-Sanz, Villegas-Perez, Bray, & Aguayo, 1988; Villegas-Perez et al., 1993), and the animals were processed 72 h later.

2.2.2. Tracing from the superior colliculi

To identify the population of RGCs contributing to the retinotectal projection, OHSt was applied to both SCi in a group of 24 Swiss or 21 C57 adult mice, from which a total of 43 or 42 retinas were analyzed, respectively. In brief, after exposing the midbrain, a small pledget of gelatin sponge (Espongostan® Film, Ferrosan A/S, Denmark) soaked in saline containing 10% OHSt in 0.9% NaCl and 10% DMSO, was applied over the entire surface of both SCi following previously described methods that are standard in our laboratory (Salinas-Navarro et al., 2009; Vidal-Sanz et al., 1988; Wang et al., 2000).

2.3. Histology and retinal examination

Mice were deeply anesthetized, perfused transcardially through the ascending aorta with saline and then with 4% paraformaldehyde in 0.1 M phosphate buffer (PB) (pH 7.4). Special care was taken to maintain the orientation of each eye, and right after deep anesthesia and before perfusion fixation a suture was placed on the superior pole of each eye. Upon dissection of the eyeball, the rectus muscle insertion into the superior part of the eye and the nasal caruncle were used as additional landmarks. Both retinas were dissected and prepared as flattened whole-mounts by making four radial cuts (the deepest one in the superior pole), post-fixed

for an additional hour, rinsed in 0.1 M PB, mounted vitreal side up on subbed slides and covered with anti-fading mounting media containing 50% glycerol and 0.04% p-phenylenediamine in 0.1 M sodium carbonate buffer (pH 9).

Retinas were photographed under a fluorescence microscope (Axioscop 2 Plus; Zeiss Mikroskopie, Jena, Germany) equipped with an ultraviolet (BP 365/12, LP 397) filter that allows the observation of the white–gold OHSt fluorescence. The microscope was also equipped with a digital high-resolution camera (ProgRes™ C10, Jenoptik, Jena, Germany) and a computer-driven motorized stage (ProScan™ H128 Series, Prior Scientific Instruments, Cambridge, UK), connected to an image analysis computer program (IPP 5.1 for Windows®; Media Cybernetics, Silver Spring, MD, USA) with a microscope controller module (Scope-Pro® 5.0 for Windows®; Media Cybernetics, Silver Spring, MD, USA).

Retinal whole-mount reconstructions were obtained with retinal multi-frame acquisitions photographed in a raster scan pattern where the frames were captured contiguously side-by-side with no gap or overlap between them with a ×20 objective (Plan-Neofluar, 20×/0.50; Zeiss Mikroskopie, Jena, Germany). Single frames were focused manually prior to the capture of the image, which were then fed into the image analysis program. A scan area was defined to cover completely the whole retina, this area consists of a matrix of m frames in columns and n frames in rows, where the total number of frames in the scan area is indicated by frames in columns times frames in rows ($m \times n$). Usually 140 images, measuring each (0.2161 mm^2) at a resolution of (300 dots per in.), were taken for each mouse retina.

The images taken for each retina were saved in a folder as a set of 24-bit color image pictures and later, these images can be combined automatically into a single tiled high-resolution composite image of the whole retina using IPP® for Windows®. Reconstructed images were further processed using image-editing software (Adobe Photoshop® CS; ver 8.0.1, Adobe Systems, Inc., San Jose, CA) when needed to produce printouts.

2.4. Image analysis

All individual images taken from every retina were processed following a specific cell counting subroutine that was developed to automate repetitive tasks and thus to count FG-labeled RGCs in mice retinas. These subroutines differ slightly from our previously described subroutines to count rat RGCs (Nadal-Nicolás et al., 2009; Salinas-Navarro et al., 2009) and have been outlined in a schematic figure (Fig. 1). In brief, we used IPP macro language to apply a sequence of filters and transformations to each image in order to clarify cell limits and separate individual cells for automatic cell counting. In a first step, the images were converted to 8-bit gray scale images. Illumination aberrations caused by the microscope optics were removed by the software flatten enhancement filter which evens out the background variations. This was followed by enhancement of the edges of the cells using the large spectral filter edge+ command, which extracts positive edges (in this case fluorescent stained bright cells) from the dark background. A setting of 8% (kernel size 20 × 20) was sufficient to enhance the cell edges making detection simpler. Large spectral filters were used where large kernels were required and cut down on the processing overheads. Small artifacts and noise were removed by running three passes of the median enhancement filter (kernel size 3 × 3). Cell clusters were then separated by two passes of the watershed split morphological filter which erodes objects until they split and then dilates them until they do not touch. The cells in each image were counted using predetermined parameters to exclude objects that were larger than 300 μm^2 or smaller than 7 μm^2. These parameters correspond to the largest or smallest individual FG-labeled object detected as RGC (Fig. 1). Finally, each count was exported by dynamic data exchange to a spreadsheet (Microsoft® Office Excel 2003, Microsoft Corporation, Redmond, WA, USA).

Retinal area was measured on the tiled high-resolution photomontage image of the whole retina with the IPP® program. For that purpose, a spatial calibration must be applied to the image based on its capture settings and produced by calibrating the stage.

2.5. Pseudo-colored density maps

The pattern of RGC distribution over the entire retina was analyzed with isodensity maps. Cell densities were calculated and represented as a filled contour plot graph. Every captured frame was divided in an equal number of 36 rectangular areas of interest (AOI). These AOI were counted (using the previously described cell counting subroutine as above) and data was exported and saved to a spreadsheet computer program (Microsoft® Office Excel 2003, Microsoft Corporation, Redmond, WA). Finally the data were represented as a filled contour plot using graphing software (SigmaPlot® 9.0 for Windows®, Systat Software, Inc., Richmond, CA) that constructs pseudo-colored isodensity maps in a scale of 45 different steps (each of 125) ranging from 0 to 5625 cells/mm^2. This upper limit was chosen on the basis of the earlier animals analyzed in the present studies, that showed mean highest densities around this value. Cell density calculating error due to frames not fully occupied by retinal tissue on the whole retina contour is minimized by the high number of AOI with a relatively small size in each frame and by the almost absence of RGCs in the retinal periphery.

2.6. Method validation

To validate the counting method, a total of 26,606 RGCs labeled by the application of OHSt to both SCi in Swiss and C57 mice, in 41 randomly selected digital images covering different density rates of 4 different normal retinas were counted manually by four different experienced investigators in a masked fashion. These were also counted automatically and the results compared to those obtained manually (Fig. 2).

2.7. Statistics

The statistical analysis of the differences between groups of retinas or groups of animals was done using non-parametric ANOVA tests using Statistix® V1.0 for Windows 95 software: the Kruskal-Wallis test was used to compare more than two groups and the Mann–Whitney test was used when comparing two groups only. To compare cell counts obtained automatically with those obtained manually we used the Pearson correlation test (SigmaStat® for Windows™ Version 3.11; Systat Software, Inc., Richmond, CA, USA). Differences were considered significant when $P < 0.05$.

3. Results

The albino (Swiss) and pigmented (C57) strain of mice are commonly employed for a number of experimental approaches aimed at studying the problem of injury-induced RGC loss and its prevention, thus it was of interest to determine as a baseline for future studies, the population and spatial distribution of RGCs in these mice. There is a mean of 49,493 and 42,658 RGCs, in the albino and pigmented mice, respectively, as revealed by retrograde axoplasmic transport of OHSt from the optic nerve. The numbers of RGCs retrogradely labeled from both SCi in Swiss and C57 mice were slightly smaller (1.5% and 3.4%, respectively) but comparable to those retrogradely labeled from the optic nerves. Thus, in mice (Drager & Olsen,

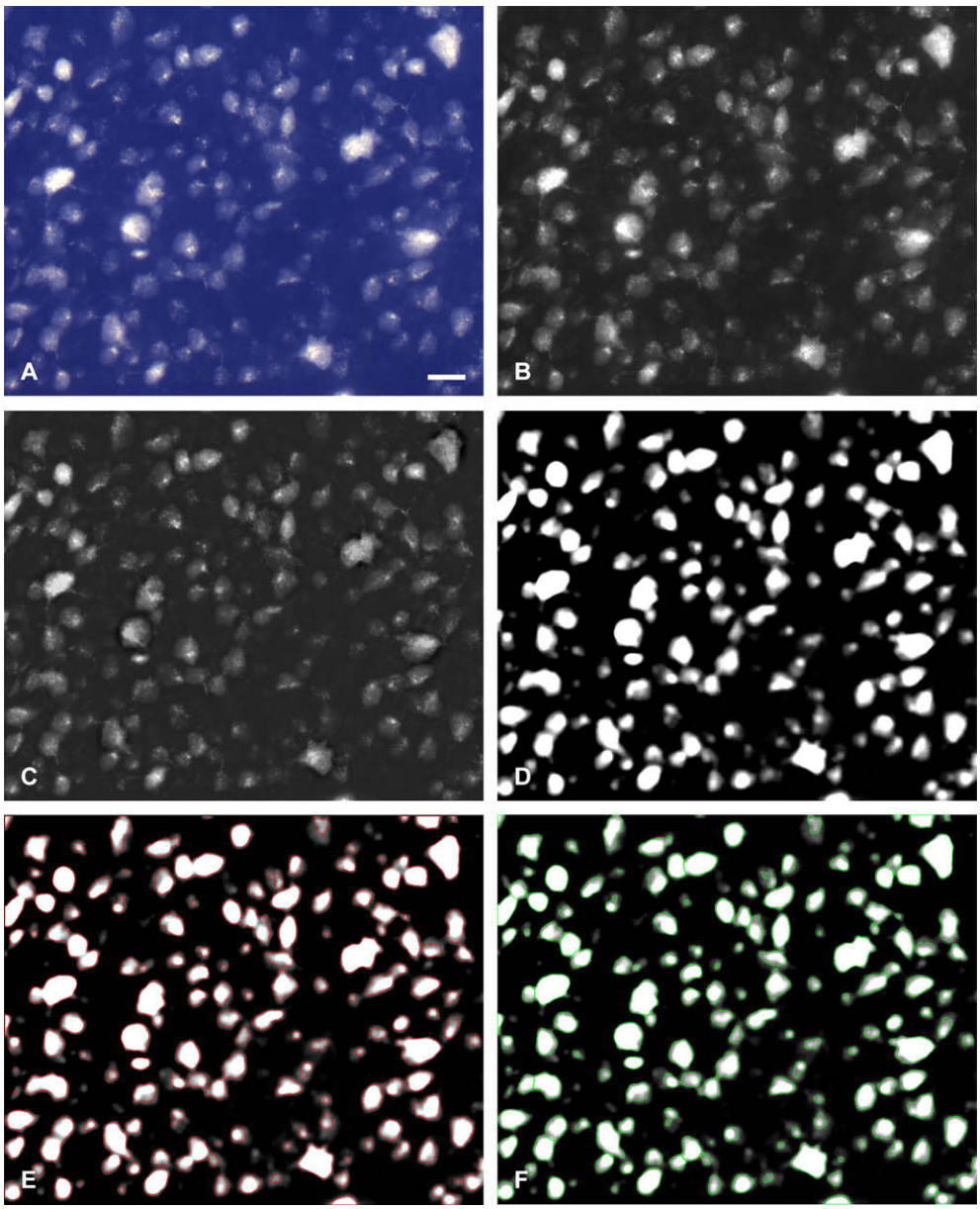

Fig. 1. Outline of automatic subroutines to count labeled retinal ganglion cells. (A) Fluorescence micrograph from a representative whole-mounted C57 mice retina, showing at high power retinal ganglion cells retrogradely labeled with OHSt applied to both SCi for 1 week prior to animal processing. The micrograph was taken on the middle region of the retina and when counted manually shows 154 labeled RGCs. (B) To count automatically this image in a first step the image was converted to 8-bit gray scale image [IpWsConvertImage(IMC_GRAY, CONV_SCALE, 0, 0, 0, 0)]. (C) Illumination aberrations were removed by the software flatten enhancement filter [IpFltFlatten(1, 20)]. (D) The edges of the cells were enhanced by using the large spectral filter edge+ command [IpLSFltApply (LF_EDGEPL,50,50,1,10)] and small artifacts and noise were removed by running three passes of the median enhancement filter [IpFltMedian(3, 3)]. (E) Cells were counted by running the counting function [IpBlbCount()]. (F) Cell clusters were then separated by two passes of the watershed split morphological filter [IpBlbSplitObjects(1)] and recounted. Scale bar for A, 20 μm.

1981), as has been shown for rats (Lund, 1965; Perry, 1981; Salinas-Navarro et al., 2009), the retinofugal system gives rise to a massive retinotectal projection. There were significant differences between the total numbers of RGCs in the albino and pigmented mice, which probably reflect genetic differences (Williams, Strom, Rice, & Goldowitz, 1996). The spatial distribution of RGCs within the retina was examined with filled contour plot graphs and these provided additional direct evidence (Drager & Olsen, 1981) of a horizontal area of highest density in the dorsal retina.

3.1. Validation of cell counts

In 41 randomly selected frames from right and left retinas, 26,492 OHSt-labeled RGCs were counted manually by four different investigators blinded to the conditions compared. These results were plotted against the counts obtained automatically with the analysis program and revealed a strong correlation between both methods (Pearson correlation test, $R = 0.995$; $P < 0.0001$) (Fig. 2), thus indicating the accuracy of the automatic counting.

3.2. RGCs in Swiss and C57 mice

The mice retinas showed RGCs labeled (Fig. 1A) with bright punctate and diffuse white or yellow–gold OHSt fluorescence delineating their soma and occasionally the proximal aspects of their primary processes (Lafuente López-Herrera, et al., 2002; Lafuente, Villegas-Pérez, et al., 2002; Peinado-Ramon et al., 1996; Sellés-Navarro et al., 1996; Vidal-Sanz et al., 2001). Labeled RGCs

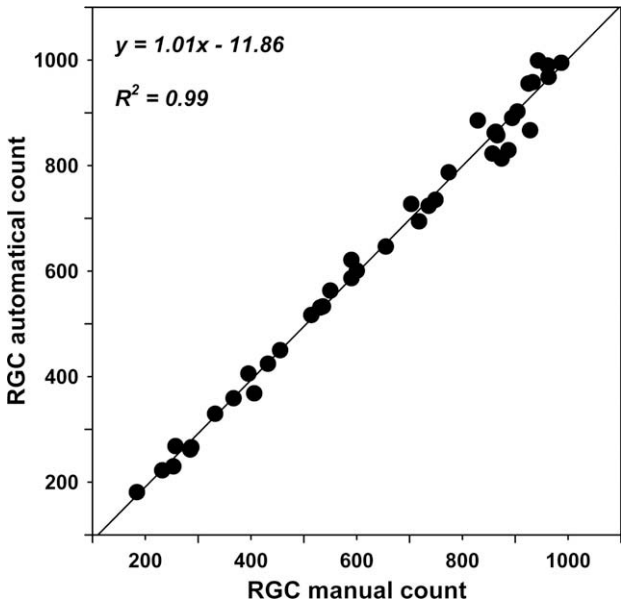

Fig. 2. Validation of automated RGC counting. The numbers of retinal ganglion cells counted manually were correlated to those obtained automatically in 40 randomly selected frames with various RGC densities. The dark line is the line that corresponds to best fit for the data, for which the equation and correlation coefficient are displayed on the graph.

were observed throughout the RGC layer of the retina with clusters containing higher cell densities in the central regions of the retina (Fig. 3A). Small numbers of displaced OHSt-labeled RGCs, also called Dogiel's cells (Dogiel, 1888), were observed when focusing the inner nuclear layer of the retina but these were not taken into account for the present study.

3.2.1. Retinofugal population of RGCs

Three days after tracer application to the intraorbital aspect of the ON, the mean total number of retrogradely labeled RGCs was 49,493 ± 3936 (n = 18; mean ± SD) (Table 1) or 42,658 ± 1540 (n = 10; mean ± SD) (Table 2) for Swiss or C57 mice, respectively. There were no significant differences between the numbers of OHSt-labeled RGCs obtained in the right retinas when compared to their fellow contralateral left retinas for the Swiss (*Mann–Whitney test, P = 0.5962*) (Table 1) or C57 mice retinas (Mann–Whitney test, *P = 0.5309*) (Table 2), respectively.

3.2.2. Retinotectal population of RGCs

Seven days after OHSt application to the SCi the numbers of labeled RGCs were 48,733 ± 3954 (n = 43; mean ± SD) (Table 3) or 41,192 ± 3395 (n = 42; mean ± SD) (Table 4), in the Swiss or C57 mice retinas, respectively. There were no differences between the numbers of labeled RGCs obtained in the right retinas when compared to their fellow contralateral left retinas in the Swiss (*Mann–Whitney test, P = 0.9129*) (Table 3) or C57 (*Mann–Whitney test, P = 0,1249)* (Table 4) mice, respectively. Overall, the values obtained were quite consistent within each group o retinas analyzed.

3.3. Areas and RGC densities

In the group of Swiss mice, the areas of the retinas varied between 12.5 and 22.7 mm^2 with a mean value of 16 ± 2.3 (n = 43; mean ± SD) for the group of Swiss mice labeled from the SCi and between 12.4 and 20.8 mm^2 with a mean value of 16 ± 2.3 (n = 18; mean ± SD) for the group of Swiss mice labeled from the ONs. (Tables 1 and 3). In these retinas, the mean densities of labeled RGCs varied between 2280 and 3898 with a mean of 3083 ± 378 (n = 43; mean ± SD) (Table 1) for the group of Swiss mice labeled from the SCi and between 2616 and 3771 with a mean of 3122 ± 277 (n = 18; mean ± SD) (Table 3) for those labeled from the ONs.

In the groups of C57 mice, the areas of the retinas varied between 12.8 and 17 mm^2 with a mean value of 14.6 ± 0.8 (n = 42; mean ± SD) (Table 2) for the group of C57 mice labeled from the SCi and between 12.8 and 16.2 mm^2 with a mean value of 14.5 ± 1 (n = 10; mean ± SD) (Table 4) for the group of C57 mice labeled from the ONs. In these retinas, the densities of labeled RGCs varied between 2044 and 3549 with a mean of 2821 ± 281 (n = 42; mean ± SD) (Table 2) for the group of C57 mice labeled from the SCi and between 2693 and 3155 with a mean of 2949 ± 143 (n = 10; mean ± SD) (Table 4) for the group of C57 mice labeled from the ONs.

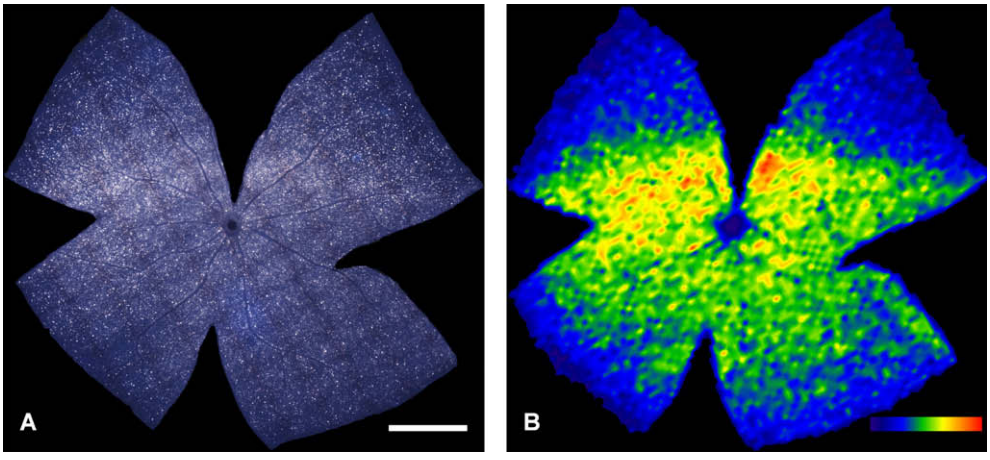

Fig. 3. Retinal whole-mount of a representative Swiss mice right retina showing RGCs retrogradely labeled with OHSt applied to both SCi for 1 week prior to animal processing and its corresponding filled contour plot pseudo-color isodensity map. (A) Whole-mount reconstruction prepared with the aid of a motorized stage on a photomicroscope with a high-resolution camera connected to an image analysis system with an automatic frame grabber device (Image-Pro® Plus, V5; Media Cybernetics, Silver Spring, MD, USA). Retinal multi-frame acquisitions were photographed in a raster scan pattern where the frames were captured contiguously side-by-side with no gap or overlap between them. Intensely labeled RGCs are distributed throughout the retina, but present higher densities in a region along the naso-temporal axis on the superior retina. (B) Isodensity map constructed for this retina, represented as a filled contour plot generated by assigning to each one of the 36 subdivisions of each individual frame a color code according to its RGCs density value within a 45-step color scale range from 0 (dark blue) to 5625 or higher RGCs/mm^2 (red). For all retinas the superior pole is orientated at the 12 o'clock orientation. This retina has 47,823 OHSt-labeled RGCs. Scale bar = 1 mm.

Table 1
Number of ganglion cells retrogradely labeled from the superior colliculi (Swiss mice).

Animal #	Right retina			Left retina		
	Cells	Area (mm^2)	Mean cell density (cells/mm^2)	Cells	Area (mm^2)	Mean cell density (cells/mm^2)
1	–	–	–	48,383	15.2	3175
2	45,398	12.8	3536	46,716	13.2	3547
3	50,712	13.0	3898	50,362	14.0	3605
4	48,358	14.0	3457	50,947	14.4	3538
5	45,961	14.9	3085	48,613	13.8	3525
6	44,332	12.5	3538	44,345	12.5	3548
7	47,748	14.0	3411	47,880	13.8	3470
8	54,940	15.2	3622	51,620	14.0	3700
9	49,949	18.0	2780	44,215	15.8	2806
10	49,871	15.4	3234	51,616	16.4	3140
11	51,300	16.1	3178	52,924	16.4	3223
12	46,158	14.5	3188	44,306	16.1	2760
13	45,994	15.8	2907	–	–	–
14	44,700	16.1	2776	43,979	15.0	2923
15	44,246	15.6	2837	39,281	15.1	2598
16	52,579	20.5	2563	51,353	19.7	2601
17	56,143	20.6	2723	56,721	22.7	2502
18	45,150	15.5	2907	–	–	–
19	–	–	–	49,956	16.6	3002
20	50,128	17.2	2911	50,108	17.1	2934
21	52,414	17.9	2928	40,513	17.9	2280
22	51,156	16.4	3121	52,321	17.2	3037
23	52,248	18.0	2901	52,031	18.5	2819
24	47,823	20.4	2345	–	–	–
Mean	48969[b]	16.1	3084	48485[b]	16	3082
SD	3502	2.4	378	4370	2.4	414
n	22	22	22	21	21	21
Mean[a]	48,733	16.0	3083			
SD[a]	3954	2.3	378			
n	43	43	43			

[a] Data from both retinas.
[b] Not significantly different (Mann–Whitney Test, $P = 0.913$).

Table 2
Number of ganglion cells retrogradely labeled from the optic nerve (Swiss mice).

Animal #	Right retina			Left retina		
	Cells	Area (mm^2)	Mean cell density (cells/mm^2)	Cells	Area (mm^2)	Mean cell density (cells/mm^2)
1	51,835	16.8	3080	49,182	16.2	3042
2	50,044	16.7	2993	–	–	–
3	49,809	16.4	3035	49,298	17.7	2784
4	52,620	18.9	2792	54,011	18.4	2942
5	56,276	19.2	2937	54,410	20.8	2616
6	49,042	14.2	3444	46,723	12.4	3771
7	48,389	14.6	3319	49,251	15.0	3292
8	–	–	–	48,777	14.4	3387
9	49,539	14.9	3325	49,824	15.3	3261
10	40,686	13.2	3078	41,151	13.3	3106
Mean	49804[b]	16.1	3111	49181[b]	15.9	3133
SD	4180	2.0	210	3902	2.7	344
n	9	9	9	9	9	9
Mean[a]	49,493	16.0	3122			
SD[a]	3936	2.3	277			
n	18	18	18			

[a] Data from both retinas.
[b] Not significantly different (Mann–Whitney Test, $P = 0.596$).

3.4. Topography of RGCs

Upon fluorescence microscopic examination of the retinas, it was clear that OHSt-labeled RGCs were not uniformly distributed throughout the retina, but rather tended to concentrate in the central retina compared to the periphery (Figs. 3 and 4). Within the many retinas examined, there was certain variability in the location of the region containing the highest RGC density, but there was a clear tendency for this high-density region to localize in the superior retina, forming a horizontally oriented area extending naso-temporally, approximately 1 mm dorsal to the optic disk, adopting the form of a visual streak.

This high-density area was analyzed in depth using filled contour plot graph to construct colored isodensity maps in a scale of 45 different steps (each of 125) ranging from 0 to 5625 (Figs. 3 and 4). These detailed maps showed a region with highest density located in the superior retina, with RGC densities falling off rapidly from this area towards the superior and inferior retina, but

Table 3
Number of ganglion cells retrogradely labeled from the superior colliculi (C57 mice).

Animal #	Right retina			Left retina		
	Cells	Area (mm^2)	Mean cell density (cells/mm^2)	Cells	Area (mm^2)	Mean cell density (cells/mm^2)
1	41,096	13.8	2978	43,072	14.5	2962
2	43,841	15.0	2921	44,361	15.5	2858
3	46,173	13.0	3549	43,059	14.7	2935
4	39,509	12.8	3084	45,416	13.8	3303
5	42,978	14.7	2926	45,033	14.8	3037
6	38,810	14.8	2629	40,171	14.3	2817
7	41,502	13.6	3045	40,027	13.2	3032
8	40,924	13.6	3005	47,259	16.0	2963
9	46,123	14.3	3234	45,271	14.3	3168
10	44,906	14.3	3151	45,920	15.8	2903
11	41,006	14.6	2809	41,184	14.2	2892
12	40,767	14.8	2753	42,089	15.0	2810
13	33,201	14.7	2262	36,291	14.8	2457
14	38,326	15.2	2525	41,880	16.3	2574
15	41,519	15.1	2744	42,266	15.0	2812
16	40,675	14.7	2773	–	–	–
17	–	–	–	40,584	15.1	2688
18	35,708	14.9	2397	37,949	15.0	2528
19	38,656	14.8	2617	39,359	15.0	2629
20	38,813	14.7	2635	40,138	14.8	2719
21	31,952	15.6	2044	38,421	13.1	2931
22	39,451	14.3	2761	44,362	17.0	2613
Mean	40283[b]	14.4	2802	42101[b]	14.9	2840
SD	3658	0.7	340	2916	0.9	212
n	21	21	21	21	21	21
Mean[a]	41,192	14.6	2821			
SD[a]	3395	0.8	281			
n	42	42	42			

[a] Data from both retinas.
[b] Not significantly different (Mann–Whitney Test, $P = 0.125$).

Table 4
Number of ganglion cells retrogradely labeled from the optic nerve (C57 mice).

Animal #	Right retina			Left retina		
	Cells	Area (mm^2)	Mean cell density (cells/mm^2)	Cells	Area (mm^2)	Mean cell density (cells/mm^2)
1	42,185	14.1	3002	40,288	12.8	3155
2	41,506	13.8	3014	42,417	15.8	2693
3	45,945	16.2	2841	41,554	14.1	2958
4	43,479	15.3	2844	42,347	15.0	2829
5	43,188	14.1	3065	43,674	14.1	3089
Mean	43261[b]	14.7	2953	42056[b]	14.3	2945
SD	1695	1.0	104	1246	1.1	188
n	5	5	5	5	5	5
Mean[a]	42,658	14.5	2949			
SD[a]	1540	1.0	143			
n	10	10	10			

[a] Data from both retinas.
[b] Not significantly different (Mann–Whitney Test, $P = 0.531$).

doing so more pronouncedly on the superior retina, with a clear gradient toward the periphery (Fukuda, 1977; McCall, Robinson, & Dreher, 1987; Perry, 1981; Schober & Gruschka, 1977). This region had the highest individual densities; the mean for these highest densities were 5959 ± 495 ($n = 43$; mean ± SD) or 5851 ± 430 ($n = 42$; mean ± SD) for Swiss or C57 mice, respectively, when OHSt was applied to both SCi and 6290 ± 605 ($n = 18$; mean ± SD) or 6352 ± 319 ($n = 9$; mean ± SD) for the Swiss or C57 mice, respectively, when OHSt was applied to the optic nerve. The difference between central and peripheral retina varied but in general, there is a factor of 35–38. These values are comparable to those obtained in our laboratory for adult albino and pigmented rats, where densities differed by a factor of 33–34 (Salinas-Navarro et al., 2009).

4. Discussion

The Swiss and C57 strain of mice are commonly employed for a number of experimental approaches aimed at studying the problem of injury-induced RGC loss and its prevention, thus it was of interest to determine as a baseline for future studies, the population of RGCs in these mice to compare with mice undergoing experimental manipulations. The need for modern accurate methods to identity a specific population of neurons (e.g., RGCs) is highlighted by the fact that numbers of ganglion cells among diverse types of mice have been reported to be highly variable, with a range between 32,000 and 87,000 (Williams et al., 1996).

Identification of RGCs within the RGC layer is not a simple task. Classic morphological criteria or molecular markers have not been

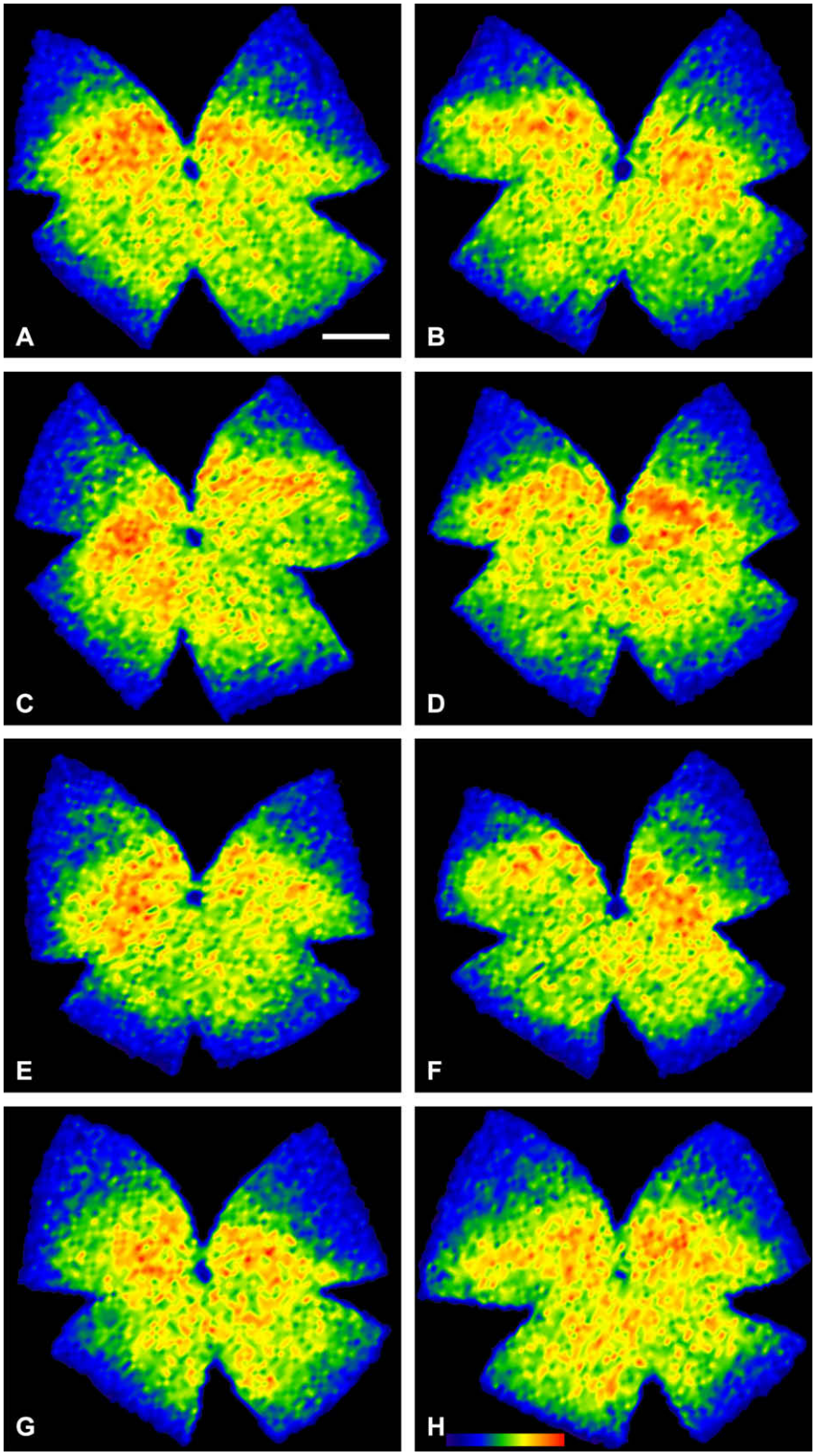

Fig. 4. Filled contour plots showing densities of RGCs in whole-mounts from both right (left column, A,C,E,G) and left (right column, B,D,F,H) retinas in three representative Swiss (AB,CD,EF) and one C57 (GH) mice in which OHSt had been applied to both superior colliculi for 1 week prior to animal processing. Maps are represented as filled contour plots generated by assigning to each one of the 36 subdivisions of each individual frame a color code according to its RGCs density value within a 45-step color scale range from 0 (dark blue) to 5625 or higher RGCs/mm^2 (red). The maps show the typical high-density distribution along a naso-temporal streak in the superior retina. For all retinas the superior pole is orientated at the 12 o'clock orientation. Scale bar = 1 mm.

proven to reliably distinguish RGCs from the many amacrine cells that are displaced into the rodent RGC layer (Drager & Olsen, 1981; Jeon et al., 1998; Perry, 1981; Perry et al., 1983; Schmidt et al., 2001) even though recent stereological approaches (Fileta et al.,

2008) as well as some molecular markers for RGCs (Nadal-Nicolás et al., 2009; Quina et al., 2005; Soto et al., 2008) look promising. Indeed, displaced amacrine cells and small RGCs overlap in size, thus making it difficult to distinguish these classes of retinal neurons (Villegas-Perez et al., 1988; Villegas-Perez et al., 1993). For this reason, identification of RGCs in the rodent retina has relied on the use of retrogradely transported tracers applied to the optic nerves, optic tracts or to their main target regions in the brain (Salinas-Navarro et al., 2009; Vidal-Sanz et al., 1988; Villegas-Perez et al., 1993; Wang et al., 2000). Our previous work requiring quantitative estimation of the population of retinal ganglion cells (RGC) has consisted of manual counts of identified retrogradely labeled RGCs from printed photographs from standard regions of the retina that only comprised a small portion of the retina. This method is not only tedious and time consuming but also requires expertise from the investigator to identify RGCs.

Using a retrogradely transported neuronal tracer to identify the RGC population and a methodology to count labeled RGCs (Danias et al., 2002; Danias et al., 2003; Salinas-Navarro et al., 2009), in the present study we have quantified the population of RGCs giving rise to the retinofugal and retinotectal projection, respectively, and we have also constructed filled contour plot graphs to demonstrate their spatial distribution within the retina, in Swiss albino and C57 pigmented adult mice. In performing the task of counting the number of RGCs, compared to manual counting the present method takes advantage of commercially available software to do the job automatically. Moreover it is reproducible; indeed the total counts of RGCs obtained in different retinas of our groups of albino or pigmented mice were comparable (Tables 1–4). We anticipate that this counting procedure will be useful in normal and in experimental conditions in which neuronal tracers may be applied efficiently after injury (García-Ayuso et al., 2008; Marco-Gomariz, Hurtado-Montalbán, Vidal-Sanz, Lund, & Villegas-Pérez, 2006; Salinas-Navarro et al., 2006; Salinas-Navarro et al., 2009; Schnebelen et al., 2007; Schnebelen et al., 2008; Vidal-Sanz, De la Villa, et al., 2007; Vidal-Sanz, Salinas-Navarro, et al., 2007). The present studies, however, could not analyze the size of the cell somas due to the transformations imposed to the OHSt-labeled RGCs in the analysis process. Neither did we take into account the displaced RGCs observed in the inner nuclear layer of the retina, which accounts for approximately 1–2% of the RGC population in mice (Drager & Olsen, 1981), is smaller in albinos compared to pigmented mice (Drager & Olsen, 1980) and may be responsible for the decreased uncrossed projection in albinos as compared to pigmented mice (Balkema & Drager, 1990).

Overall, the population of RGCs labeled from the ONs, and thus contributing to the retinofugal projection, was slightly greater (1.5% for Swiss and 3.4% for C57 mice, respectively) than the population of RGCs labeled from both SCi, and thus contributing to the retinotectal projection, but in both cases the differences were not significant (Swiss mice, *Mann–Whitney test, P = 0.5426; C57 mice, Mann–Whitney test, P = 0.1066*). This finding is in agreement with previous studies and provides additional evidence towards the massive projection from the retina towards the tecta (Drager & Olsen, 1980; Drager & Olsen, 1981; Linden & Perry, 1983; Lund, 1965; Lund, 1969; Lund, Land, & Boles, 1980).

In our study the population of RGCs was greater in Swiss than in C57 mice. This was the case for RGCs giving rise to the retinofugal (*Mann–Whitney test, P = 0.0006*) or the retinotectal (*Mann–Whitney test, P = 0.0000*) projection. This finding is in agreement with previous studies and may reflect a genetic difference between albino and pigmented mice (Fukuda, Sugimoto, & Shirokawa, 1982; Williams et al., 1996).

The total numbers of RGCs obtained in our experiments from counts of OHSt-labeled RGCs in wholemounts are comparable to other studies that have investigated the numbers of RGCs in albino or pigmented mice counting ON axons (Cenni et al., 1996; Howell et al., 2007; Jeon et al., 1998; Mabuchi, Lindsey, Aihara, Mackey, & Weinreb, 2004; Parson, Dhillon, Findlater, & Kaufman, 1995; Williams et al., 1996) or using RGC markers (Bernstein, Guo, Slater, Puche, & Kelman, 2007). For instance, in C57/BL6 mice Jeon and colleagues (1998) and Cenni and colleagues (1996), counting ON axons found a total number of approximately 44,860 ± 3125 and 45,400 ± 4000, respectively. Our results are however somewhat smaller than those reported by others using retrograde tracers to label RGCs (Danias et al., 2003; Schmidt et al., 2001) or counting ON axons (Zhou, Strom, Giguere, & Williams, 2001). For instance, Danias and colleagues (2003) using a similar approach found in C57/BL6 mice a total number of RGCs of 84,027 ± 2171, which is larger than that found in our study. There are several possible explanations for these differences; the different regions and number of areas examined, the tracers employed and their mode of application, or the methods employed to estimate the total RGC population. Overall, the more likely explanation may relate to the different strains employed for the studies. Williams and colleagues (1996) have shown that there are large variations in the total numbers of RGCs in mice of different species, subspecies and strains (with a mean of 58,500 ± 7800 with a range from 32,000 to 87,000), and that these are genetically controlled.

The values obtained for the densities of RGCs in the groups of Swiss or C57 mice are within the range reported for albino or pigmented mice in previous studies from other independent laboratories using retrograde tracers to label RGCs (Inoue, Hosokawa, Morigiwa, Ohashi, & Fukuda, 2002; Murphy, Franklin, Rafuse, & Clarke, 2007; Robinson & Madison, 2004). Nevertheless, when central regions of the retina are sampled, the densities of FG-labeled RGCs tend to be significantly higher. This is reflected in previous studies from this (Wang et al., 2000) and other laboratories (Buckingham et al., 2008; Haustead et al., 2008; Jakobs et al., 2005; Levkovitch-Verbin et al., 2000; Schmidt et al., 2001) and this may be due to the different RGC distribution throughout the retina, with highest densities in central regions (see below). Moreover, the eyes of mice grow through early adult life, thus changing their absolute density (Jeon et al., 1998), something we could only control for the present study by using animals of comparable weight. Although it is unlikely, we cannot rule out the possibility that the mice used in our experiments had similar weights but different ages, and this would explain the variations observed in the areas of the retinas in some of these mice.

The presence in the dorsal retina of an elongated region of elevated RGC density horizontally oriented along the naso-temporal axis, resembles a visual streak. This regional specialization of the RGC distribution in the retina, which has its counterpart on the visual field representation in the superior colliculus (Drager & Hubel, 1976), was observed by others in the Syrian hamster (Métin et al., 1995), in the rat (Jeffery, 1985; Reese & Cowey, 1986) and in pigmented (C57BL/6J) mice (Drager & Olsen, 1981), and also in this Laboratory for the pigmented non-dystrophic RCS rat (Marco-Gomariz et al., 2006), the Sprague-Dawley and the PVG rat (Salinas-Navarro et al., 2009). Previous studies have pointed out the presence of visual streaks with very shallow gradients, such as those presented in this work for mice, in the guinea pig (do Nascimento, do Nascimento, Damasceno, & Silveira, 1991) or with extremely pronounced gradients in larger rodents such as the agouti and the capybara (Silveira et al., 1989; Silveira et al., 1989).

Our present findings are in contrast to previous reports (Danias et al., 2003), but in our analysis we did not find evidence for the visual streak until detailed density maps, based on small frames, were constructed (Figs. 3 and 4). Indeed, our filled contour plots constructed on the base of the analysis of the 36 areas of interest in which every frame was divided, implies an increase in resolution of approximately 15 times, when compared to such study (Danias

et al., 2003). This was also the case for our previous study in which we did examine the retinal distribution of RGCs in adult pigmented and non-pigmented rat retinas (Salinas-Navarro et al., 2009). Nevertheless, our maps show that the highest density clusters of RGCs tended to localize on the superior temporal quadrant in most retinas, and this is in agreement with previous studies in range of rodents, including Syriam hamster (Métin et al., 1995) rat (Dreher et al., 1985; Fukuda, 1977; Jeffery, 1985; McCall et al., 1987; Perry, 1981; Reese & Cowey, 1986; Schober & Gruschka, 1977) and mice (Drager & Olsen, 1981; Jakobs et al., 2005; Jeon et al., 1998).

Acknowledgments

The technical contribution of Isabel Cánovas and José M. Bernal is greatly acknowledged.

This work was supported by research grants from the Regional Government of Murcia, Fundación Séneca 02989/PI/05, 05703/PI/07, 04446/GERM/07; Spanish Ministry of Education and Science SAF-2005-04812; and Spanish Ministry of Health ISCIII: FIS PIO06/0780 and RD07/0062/0001; and an unrestricted grant from Allergan Inc.

References

Agudo, M., Pérez-Marín, M. C., Lönngren, U., Sobrado, P., Conesa, A., Cánovas, I., et al. (2008). Time course profiling of the retinal transcriptome after optic nerve transection and optic nerve crush. *Molecular Vision, 14*, 1050–1063.

Agudo, M., Pérez-Marín, M. C., Sobrado-Calvo, P., Lönngren, U., Salinas-Navarro, M., Cánovas, I., et al. (2009). Immediate upregulation of proteins belonging to different branches of the apoptotic cascade in the retina after optic nerve transection and optic nerve crush. *Investigative Ophthalmology and Visual Science, 50*, 424–431.

Avilés-Trigueros, M., Mayor-Torroglosa, S., García-Avilés, A., Lafuente, M. P., Rodríguez, M. E., Miralles de Imperial, J., et al. (2003). Transient ischemia of the retina results in massive degeneration of the retinotectal projection: Long-term neuroprotection with brimonidine. *Experimental Neurology, 184*, 767–777.

Avilés-Trigueros, M., Sauvé, Y., Lund, R. D., & Vidal-Sanz, M. (2000). Selective innervation of retinorecipient brainstem nuclei by retinal ganglion cell axons regenerating through peripheral nerve grafts in adult rats. *Journal of Neuroscience, 20*, 361–374.

Balkema, G. W., & Drager, U. C. (1990). Origins of uncrossed retinofugal projections in normal and hypopigmented mice. *Visual Neuroscience, 4*, 595–604.

Bernstein, S. L., Guo, Y., Slater, B. J., Puche, A., & Kelman, S. E. (2007). Neuron stress and loss following rodent anterior ischemic optic neuropathy in double-reporter transgenic mice. *Investigative Ophthalmology and Visual Science, 48*, 2304–2310.

Buckingham, B. P., Inman, D. M., Lambert, W., Oglesby, E., Calkins, D. J., Steele, M. R., et al. (2008). Progressive ganglion cell degeneration precedes neuronal loss in a mouse model of glaucoma. *Journal of Neuroscience, 28*, 2735–2744.

Cenni, M. C., Bonfanti, L., Martinou, J. C., Ratto, G. M., Strettoi, E., & Maffei, L. (1996). Long-term survival of retinal ganglion cells following optic nerve section in adult bcl-2 transgenic mice. *European Journal of Neuroscience, 8*, 1735–1745.

Cheunsuang, O., & Morris, R. (2005). Astrocytes in the arcuate nucleus and median eminence that take up a fluorescent dye from the circulation express leptin receptors and neuropeptide Y Y1 receptors. *Glia, 52*, 228–233.

Chidlow, G., Casson, R., Sobrado-Calvo, P., Vidal-Sanz, M., & Osborne, N. N. (2005). Measurement of retinal injury in the rat after optic nerve transection: An RT-PCR study. *Molecular Vision, 11*, 387–396.

Danias, J., Lee, K. C., Zamora, M. F., Chen, B., Shen, F., Filippopoulos, T., et al. (2003). Quantitative analysis of retinal ganglion cell (RGC) loss in aging DBA/2NNia glaucomatous mice: Comparison with RGC loss in aging C57/BL6 mice. *Investigative Ophthalmology and Visual Science, 44*, 5151–5162.

Danias, J., Shen, F., Goldblum, D., Chen, B., Ramos-Esteban, J., Podos, S. M., et al. (2002). Cytoarchitecture of the retinal ganglion cells in the rat. *Investigative Ophthalmology and Visual Science, 43*, 587–594.

do Nascimento, J. L. M., do Nascimento, R. S. V., Damasceno, B. A., & Silveira, L. C. L. (1991). The neurons of the retinal ganglion cell layer of the guinea pig: Quantitative analysis of their distribution and size. *Brazilian Journal of Medical and Biological Research, 24*, 199–214.

Dogiel, A. S. (1888). Über das Verhalten der nervösen Elemente in der retina der Ganoiden, Reptilien, Vögel und Säugetiere. *Anatomischer Anzeiger, 3*, 133–134.

Drager, U. C., & Hubel, D. H. (1976). Topography of visual and somatosensory projections to mouse superior colliculus. *Journal of Neurophysiology, 39*, 91–101.

Drager, U. C., & Olsen, J. F. (1980). Origins of crossed and uncrossed retinal projections in pigmented and albino mice. *Journal of Comparative Neurology, 191*, 383–412.

Drager, U. C., & Olsen, J. F. (1981). Ganglion cell distribution in the retina of the mouse. *Investigative Ophthalmology and Visual Science, 20*, 285–293.

Dreher, B., Sefton, A. J., Ni, S. Y., & Nisbett, G. (1985). The morphology, number, distribution and central projections of class I retinal ganglion cells in albino and hooded rats. *Brain Behavior and Evolution, 26*, 10–48.

Fileta, J. B., Huang, W., Kwon, G. P., Filippopoulos, T., Ben, Y., Dobberfuhl, A., et al. (2008). Efficient estimation of retinal ganglion cell number: A stereological approach. *Journal of Neuroscience Methods, 170*, 1–8.

Fukuda, Y. (1977). A three-group classification of rat retinal ganglion cells: Histological and physiological studies. *Brain Research, 119*, 327–334.

Fukuda, Y., Sugimoto, T., & Shirokawa, T. (1982). Strain differences in quantitative analysis of the rat optic nerve. *Experimental Neurology, 75*, 525–532.

García-Ayuso, D., Salinas-Navarro, M., Coll-Alcaraz, L., Cánovas-Martínez, I., Bernal-Garro, J. M., Vidal-Sanz, M., et al. (2008). Characterization of the light-sensitive arciform region in the albino rat retina. *Investigative Ophthalmology and Visual Science*, 49 [E-Abstract 4395].

Haustead, D. J., Lukehurst, S. S., Clutton, G. T., Bartlett, C. A., Dunlop, S. A., Arrese, C. A., et al. (2008). Functional topography and integration of the contralateral and ipsilateral retinocollicular projections of ephrin-A-/- mice. *Journal of Neuroscience, 28*, 7376–7386.

Howell, G. R., Libby, R. T., Jakobs, T. C., Smith, R. S., Phalan, F. C., Barter, J. W., et al. (2007). Axons of retinal ganglion cells are insulted in the optic nerve early in DBA/2J glaucoma. *Journal of Cell Biology, 179*, 1523–1537.

Inoue, T., Hosokawa, M., Morigiwa, K., Ohashi, Y., & Fukuda, Y. (2002). Bcl-2 overexpression does not enhance in vivo axonal regeneration of retinal ganglion cells after peripheral nerve transplantation in adult mice. *Journal of Neuroscience, 22*, 4468–4477.

Jakobs, T. C., Libby, R. T., Ben, Y., John, S. W., & Masland, R. H. (2005). Retinal ganglion cell degeneration is topological but not cell type specific in DBA/2J mice. *Journal of Cell Biology, 171*, 313–325.

Jeffery, G. (1985). The relationship between cell density and the nasotemporal division in the rat retina. *Brain Research, 347*, 354–357.

Jeon, C. J., Strettoi, E., & Masland, R. H. (1998). The major cell populations of the mouse retina. *Journal of Neuroscience, 18*, 8936–8946.

Lafuente López-Herrera, M. P., Mayor-Torroglosa, S., Miralles de Imperial, J., Villegas-Pérez, M. P., & Vidal-Sanz, M. (2002). Transient ischemia of the retina results in altered retrograde axoplasmic transport: Neuroprotection with brimonidine. *Experimental Neurology, 178*, 243–258.

Lafuente, M. P., Villegas-Pérez, M. P., Mayor-Torroglosa, S., Aguilera, M. E., Miralles de Imperial, J., & Vidal-Sanz, M. (2002). Neuroprotective effects of brimonidine against transient ischemia-induced retinal ganglion cell death: A dose response in vivo study. *Experimental Eye Research, 74*, 181–189.

Lafuente, M. P., Villegas-Pérez, M. P., Sellés-Navarro, I., Mayor-Torroglosa, S., Miralles de Imperial, J., & Vidal-Sanz, M. (2002). Retinal ganglion cell death after acute retinal ischemia is an ongoing process whose severity and duration depends on the duration of the insult. *Neuroscience, 109*, 157–168.

Levkovitch-Verbin, H., Harris-Cerruti, C., Groner, Y., Wheeler, L. A., Schwartz, M., & Yoles, E. (2000). RGC death in mice after optic nerve crush injury: Oxidative stress and neuroprotection. *Investigative Ophthalmology and Visual Science, 41*, 4169–4174.

Linden, R., & Perry, V. H. (1983). Massive retinotectal projection in rats. *Brain Research, 272*, 145–149.

Lund, R. D. (1965). Uncrossed visual pathways of hooded and albino rats. *Science, 149*, 1506–1507.

Lund, R. D. (1969). Synaptic patterns of the superficial layers of the superior colliculus of the rat. *Journal of Comparative Neurology, 135*, 179–208.

Lund, R. D., Land, P. W., & Boles, J. (1980). Normal and abnormal uncrossed retinotectal pathways in rats: An HRP study in adults. *Journal of Comparative Neurology, 189*, 711–720.

Lund, R. D., Wang, S., Lu, B., Girman, S., Holmes, T., Sauvé, Y., et al. (2007). Cells isolated from umbilical cord tissue rescue photoreceptors and visual functions in a rodent model of retinal disease. *Stem Cells, 25*, 602–611.

Mabuchi, F., Lindsey, J. D., Aihara, M., Mackey, M. R., & Weinreb, R. N. (2004). Optic nerve damage in mice with a targeted type I collagen mutation. *Investigative Ophthalmology and Visual Science, 45*, 1841–1845.

Marco-Gomariz, M. A., Hurtado-Montalbán, N., Vidal-Sanz, M., Lund, R. D., & Villegas-Pérez, M. P. (2006). Phototoxic-induced photoreceptor degeneration causes retinal ganglion cell degeneration in pigmented rats. *Journal of Comparative Neurology, 498*, 163–179.

Mayor-Torroglosa, S., De la Villa, P., Rodríguez, M. E., López-Herrera, M. P., Avilés-Trigueros, M., García-Avilés, A., et al. (2005). Ischemia results 3 months later in altered ERG, degeneration of inner layers, and deafferented tectum: Neuroprotection with brimonidine. *Investigative Ophthalmology and Visual Science, 46*, 3825–3835.

McCall, M. J., Robinson, S. R., & Dreher, B. (1987). Differential retinal growth appears to be the primary factor producing the ganglion cell density gradient in the rat. *Neuroscience Letters, 79*, 78–84.

Métin, C., Irons, W. A., & Frost, D. O. (1995). Retinal ganglion cells in normal hamsters and hamsters with novel retinal projections I. Number, distribution, and size. *Journal of Comparative Neurology, 353*, 179–199.

Murphy, J. A., Franklin, T. B., Rafuse, V. F., & Clarke, D. B. (2007). The neural cell adhesion molecule is necessary for normal adult retinal ganglion cell number and survival. *Molecular and Cellular Neuroscience, 36*, 280–292.

Nadal-Nicolás, F., Jiménez-López, M., Sobrado-Calvo, P., Nieto-López, L., Cánovas-Martínez, I., Salinas-Navarro, M., et al. (2009). Brn3a as a marker of retinal ganglion cells: Qualitative and quantitative time course studies in naïve and optic nerve injured retinas. *Investigative Ophthalmology and Visual Science*.

Parson, S. H., Dhillon, B., Findlater, G. S., & Kaufman, M. H. (1995). Optic nerve hypoplasia in the fetal alcohol syndrome: A mouse model. *Journal of Anatomy, 186*(Pt 2), 313–320.

Peinado-Ramon, P., Salvador, M., Villegas-Perez, M. P., & Vidal-Sanz, M. (1996). Effects of axotomy and intraocular administration of NT-4, NT-3, and brain-derived neurotrophic factor on the survival of adult rat retinal ganglion cells. A quantitative in vivo study. *Investigative Ophthalmology and Visual Science, 37*, 489–500.

Perry, V. H. (1981). Evidence for an amacrine cell system in the ganglion cell layer of the rat retina. *Neuroscience, 6*, 931–944.

Perry, V. H., Henderson, Z., & Linden, R. (1983). Postnatal changes in retinal ganglion cell and optic axon populations in the pigmented rat. *Journal of Comparative Neurology, 219*, 356–368.

Prusky, G. T., Harker, K. T., Douglas, R. M., & Whishaw, I. Q. (2002). Variation in visual acuity within pigmented, and between pigmented and albino rat strains. *Behavioural Brain Research, 136*, 339–348.

Quina, L. A., Pak, W., Lanier, J., Banwait, P., Gratwick, K., Liu, Y., et al. (2005). Brn3a-expressing retinal ganglion cells project specifically to thalamocortical and collicular visual pathways. *Journal of Neuroscience, 25*, 11595–11604.

Reese, B. E. (2002). Rat retinal ganglion cell topography. *Investigative Ophthalmology and Visual Science eLetters for Danias et al, 43*, 587–594.

Reese, B. E., & Cowey, A. (1986). Large retinal ganglion cells in the rat: Their distribution and laterality of projection. *Experimental Brain Research, 61*, 375–385.

Robinson, G. A., & Madison, R. D. (2004). Axotomized mouse retinal ganglion cells containing melanopsin show enhanced survival, but not enhanced axon regrowth into a peripheral nerve graft. *Vision Research, 44*, 2667–2674.

Rodiek, R. W. (1979). Visual pathways. *Annual Reviews of Neuroscience, 2*, 193–225.

Salinas-Navarro, M., Mayor-Torroglosa, S., Holmes, T., Bernal, J. M., Cánovas, I., Aguilera, M. E., et al. (2005). Automatic quantitative analysis of retinal ganglion cells that project to the superior colliculi in adult Sprague–Dawley rats. *Investigative Ophthalmology and Visual Science, 46* [E-Abstract 271].

Salinas-Navarro, M., Mayor-Torroglosa, S., Jiménez-López, M., Avilés-Trigueros, M., Holmes, T., Lund, R. D., et al. (2009). A computerized analysis of the entire retinal ganglion cell population and its spatial distribution in adult rats. *Vision Research, 49*, 115–126.

Salinas-Navarro, M., Triviño, A., Ramírez, A. I., Salazar, J. J., Ramírez, J. M., Villegas-Pérez, M. P., et al. (2006). Long term effects of laser-induced ocular hypertension: Retrograde degeneration of retinal ganglion cells. *Investigative Ophthalmology and Visual Science, 47*.

Sasaki, H., Coffey, P., Villegas-Pérez, M. P., Vidal-Sanz, M., Young, M. J., Lund, R. D., et al. (1996). Light induced EEG desynchronization and behavioral arousal in rats with restored retinocollicular projection by peripheral nerve graft. *Neuroscience Letters, 218*, 45–48.

Sauvé, Y., Girman, S. V., Wang, S., Keegan, D. J., & Lund, R. D. (2002). Preservation of visual responsiveness in the superior colliculus of RCS rats after retinal pigment epithelium cell transplantation. *Neuroscience, 114*, 389–401.

Sauvé, Y., Girman, S. V., Wang, S., Lawrence, J. M., & Lund, R. D. (2001). Progressive visual sensitivity loss in the Royal College of Surgeons rat: Perimetric study in the superior colliculus. *Neuroscience, 103*, 51–63.

Schmidt, S. L., Vitral, R. W., & Linden, R. (2001). Effects of prenatal ionizing irradiation on the development of the ganglion cell layer of the mouse retina. *International Journal of Developmental Neuroscience, 19*, 469–473.

Schnebelen, C., Salinas-Navarro, M., Acar, N., Pasquis, B., Creuzot-Garcher, C. P., Villegas-Pérez, M. P., et al. (2007). Time course of IOP elevation, electroretinographic changes and retinal ganglion cell loss in a rat model of glaucoma induced by laser. *Investigative Ophthalmology and Visual Science, 48* [E-Abstract 206].

Schnebelen, C., Salinas-Navarro, M., Acar, N., Pasquis, B., Creuzot-Garcher, C. P., Villegas-Pérez, M. P., et al. (2008). Effect of dietary omega-3 and omega-6 fatty acids on IOP elevation, electroretinographic changes and retinal ganglion cell loss in a laser-induced rat model of glaucoma. *Investigative Ophthalmology and Visual Science, 49*, 20 [E-Abstract 5499].

Schober, W., & Gruschka, H. (1977). Retinal ganglion cells of the albino rat: A qualitative and quantitative study. *Zeitschrift für mikroskopisch-anatomische Forschung, 91*, 397–414.

Sellés-Navarro, I., Villegas-Pérez, M. P., Salvador-Silva, M., Ruiz-Gomez, J. M., & Vidal-Sanz, M. (1996). Retinal ganglion cell death after different transient periods of pressure-induced ischemia and survival intervals. A quantitative in vivo study. *Investigative Ophthalmology and Visual Science, 37*, 2002–2014.

Silveira, L. C., Picanço-Diniz, C. W., & Oswaldo-Cruz, E. (1989). The distribution and size of ganglion cells in the retinae of large Amazon rodents. *Visual Neuroscience, 2*, 221–235.

Silveira, L. C., Yamada, E. S., & Picanço-Diniz, C. W. (1989). Displaced horizontal cells and biplexiform horizontal cells in the mammalian retina. *Visual Neuroscience, 3*, 483–488.

Soto, I., Oglesby, E., Buckingham, B. P., Son, J. L., Roberson, E. D., Steele, M. R., et al. (2008). Retinal ganglion cells downregulate gene expression and lose their axons within the optic nerve head in a mouse glaucoma model. *Journal of Neuroscience, 28*, 548–561.

Vidal-Sanz, M., Avilés-Trigueros, M., Whiteley, S. J., Sauvé, Y., & Lund, R. D. (2002). Reinnervation of the pretectum in adult rats by regenerated retinal ganglion cell axons: Anatomical and functional studies. *Progress in Brain Research, 137*, 443–452.

Vidal-Sanz, M., Bray, G. M., Villegas-Perez, M. P., Thanos, S., & Aguayo, A. J. (1987). Axonal regeneration and synapse formation in the superior colliculus by retinal ganglion cells in the adult rat. *Journal of Neuroscience, 7*, 2894–2909.

Vidal-Sanz, M., De la Villa, P., Avilés-Trigueros, M., Mayor-Torroglosa, S., Salinas-Navarro, M., Alarcón-Martínez, L., et al. (2007). Neuroprotection of retinal ganglion cell function and their central nervous system targets. *Eye, 21*, S42–S45.

Vidal-Sanz, M., Lafuente, M. P., Mayor, S., de Imperial, J. M., & Villegas-Pérez, M. P. (2001). Retinal ganglion cell death induced by retinal ischemia. Neuroprotective effects of two alpha-2 agonists. *Survey of Ophthalmology, 45*, 261–267.

Vidal-Sanz, M., Lafuente, M., Sobrado-Calvo, P., Sellés-Navarro, I., Rodríguez, E., Mayor-Torroglosa, S., et al. (2000). Death and neuroprotection of retinal ganglion cells after different types of injury. *Neurotoxicity Research, 2*, 215–227.

Vidal-Sanz, M., Salinas-Navarro, M., Jiménez-López, M., Valiente-Soriano, F. J., García-Ayuso, D., Bernal, J. M., et al. (2007). Spatial distribution and quantitative analysis of retinal ganglion cells in adult albino rodents. *Investigative Ophthalmology and Visual Science, 48* [E-Abstract 134].

Vidal-Sanz, M., Villegas-Perez, M. P., Bray, G. M., & Aguayo, A. J. (1988). Persistent retrograde labeling of adult rat retinal ganglion cells with the carbocyanine dye dil. *Experimental Neurology, 102*, 92–101.

Vidal-Sanz, M., Villegas-Pérez, M. P., Bray, G. M., & Aguayo, A. J. (1993). The use of peripheral nerve grafts to study regeneration after CNS injury. *Neuroprotocols, 3*, 29–33.

Villegas-Pérez, M. P., Aguilera, M. E., Salinas-Navarro, M., Mayor-Torroglosa, S., Holmes, T., Bernal, J. M., et al. (2006). Retinal ganglion cells in adult albino and pigmented rats: Spatial distribution and quantitative analysis. *Investigative Ophthalmology and Visual Science, 47* [E-Abstract 3318].

Villegas-Perez, M. P., Lawrence, J. M., Vidal-Sanz, M., Lavail, M. M., & Lund, R. D. (1998). Ganglion cell loss in RCS rat retina: A result of compression of axons by contracting intraretinal vessels linked to the pigment epithelium. *Journal of Comparative Neurology, 392*, 58–77.

Villegas-Perez, M. P., Vidal-Sanz, M., Bray, G. M., & Aguayo, A. J. (1988). Influences of peripheral nerve grafts on the survival and regrowth of axotomized retinal ganglion cells in adult rats. *Journal of Neuroscience, 8*, 265–280.

Villegas-Perez, M. P., Vidal-Sanz, M., & Lund, R. D. (1996). Mechanism of retinal ganglion cell loss in inherited retinal dystrophy. *Neuroreport, 7*, 1995–1999.

Villegas-Perez, M. P., Vidal-Sanz, M., Rasminsky, M., Bray, G. M., & Aguayo, A. J. (1993). Rapid and protracted phases of retinal ganglion cell loss follow axotomy in the optic nerve of adult rats. *Journal of Neurobiology, 24*, 23–36.

Wang, S., Villegas-Pérez, M. P., Vidal-Sanz, M., & Lund, R. D. (2000). Progressive optic axon dystrophy and vascular changes in rd mice. *Investigative Ophthalmology and Visual Science, 41*, 537–545.

Whiteley, S. J., Sauvé, Y., Avilés-Trigueros, M., Vidal-Sanz, M., & Lund, R. D. (1998). Extent and duration of recovered pupillary light reflex following retinal ganglion cell axon regeneration through peripheral nerve grafts directed to the pretectum in adult rats. *Experimental Neurology, 154*, 560–572.

Williams, R. W., Strom, R. C., Rice, D. S., & Goldowitz, D. (1996). Genetic and environmental control of variation in retinal ganglion cell number in mice. *Journal of Neuroscience, 16*, 7193–7205.

Zhou, G., Strom, R. C., Giguere, V., & Williams, R. W. (2001). Modulation of retinal cell populations and eye size in retinoic acid receptor knockout mice. *Molecular Vision, 7*, 253–260.